

Enrique A. Lopez-Poveda • Alan R. Palmer
Ray Meddis
Editors

The Neurophysiological Bases of Auditory Perception



Springer

Contents

Part I Peripheral/Cochlear Processing

1 Otoacoustic Emissions Theories Can Be Tested with Behavioral Methods	3
Enrique A. Lopez-Poveda and Peter T. Johannesen	
2 Basilar Membrane Responses to Simultaneous Presentations of White Noise and a Single Tone	15
Alberto Recio-Spinoso and Enrique A. Lopez-Poveda	
3 The Influence of the Helicotrema on Low-Frequency Hearing	25
Torsten Marquardt and Christian Sejer Pedersen	
4 Mechanisms of Masking by Schroeder-Phase Complexes	37
Magdalena Wojtczak and Andrew J. Oxenham	
5 The Frequency Selectivity of Gain Reduction Masking: Analysis Using Two Equally-Effective Maskers	47
Skyler G. Jennings and Elizabeth A. Strickland	
6 Investigating Cortical Descending Control of the Peripheral Auditory System	59
Darren Edwards and Alan Palmer	
7 Exploiting Transgenic Mice to Explore the Role of the Tectorial Membrane in Cochlear Sensory Processing	69
Guy P. Richardson, Victoria Lukashkina, Andrei N. Lukashkin, and Ian J. Russell	
8 Auditory Prepulse Inhibition of Neuronal Activity in the Rat Cochlear Root Nucleus	79
Ricardo Gómez-Nieto, J.A.C. Horta-Júnior, Orlando Castellano, Donal G. Sinex, and Dolores E. López	

Part II Masking

- 9 FM Forward Masking: Implications for FM Processing** 93
Neal Viemeister, Andrew Byrne, Magdalena Wojtczak,
and Mark Stellmack
- 10 Electrophysiological Correlates of Intensity Resolution
Under Forward Masking**..... 99
Daniel Oberfeld
- 11 Neuronal Measures of Threshold and Magnitude
of Forward Masking in Primary Auditory Cortex** 111
Ana Alves-Pinto, Sylvie Baudoux, Alan Palmer,
and Christian J. Sumner
- 12 Effect of Presence of Cue Tone on Tuning of Auditory
Filter Derived from Simultaneous Masking** 121
Shunsuke Kidani and Masashi Unoki

Part III Spectral Processing and Coding

- 13 Tone-in-Noise Detection: Observed Discrepancies
in Spectral Integration**..... 133
Nicolas Le Goff, Armin Kohlrausch, Jeroen Breebaart,
and Steven van de Par
- 14 Linear and Nonlinear Coding of Sound Spectra
by Discharge Rate in Neurons Comprising the Ascending
Pathway Through the Lateral Superior Olive**..... 143
Daniel J. Tollin and Kanthaiah Koka
- 15 Enhancement in the Marmoset Inferior Colliculus:
Neural Correlates of Perceptual “Pop-Out”**..... 155
Paul C. Nelson and Eric D. Young
- 16 Auditory Temporal Integration at Threshold:
Evidence of a Cortical Origin** 167
B. Lütkenhöner

Part IV Pitch and Timbre

- 17 Spatiotemporal Characteristics of Cortical Responses
to a New Dichotic Pitch Stimulus** 181
Caroline Witton, Arjan Hillebrand, and G. Bruce Henning

18	A Temporal Code for Huggins Pitch?	191
	Christopher J. Plack, Suzanne Fitzpatrick, Robert P. Carlyon, and Hedwig E. Gockel	
19	Understanding Pitch Perception as a Hierarchical Process with Top-Down Modulation	201
	Emili Balaguer-Ballester, Nicholas R. Clark, Martin Coath, Katrin Krumbholz, and Susan L. Denham	
20	The Harmonic Organization of Auditory Cortex	211
	Xiaoqin Wang	
21	Reviewing the Definition of Timbre as it Pertains to the Perception of Speech and Musical Sounds	223
	Roy D. Patterson, Thomas C. Walters, Jessica J.M. Monaghan, and Etienne Gaudrain	
22	Size Perception for Acoustically Scaled Sounds of Naturally Pronounced and Whispered Words	235
	Toshio Irino, Yoshie Aoki, Hideki Kawahara, and Roy D. Patterson	
Part V Binaural Hearing		
23	Subcomponent Cues in Binaural Unmasking	247
	John F. Culling	
24	Interaural Correlations Between +1 and -1 on a Thurstone Scale: Psychometric Functions and a Two-Parameter Model	257
	Helge Lüddemann, Helmut Riedel, and Andre Rupp	
25	Dynamic ITDs, Not ILDs, Underlie Binaural Detection of a Tone in Wideband Noise	265
	Marcel van der Heijden and Philip X. Joris	
26	Effect of Reverberation on Directional Sensitivity of Auditory Neurons: Central and Peripheral Factors	273
	Sasha Devore, Andrew Schwartz, and Bertrand Delgutte	
27	New Experiments Employing Raised-Sine Stimuli Suggest an Unknown Factor Affects Sensitivity to Envelope-Based ITDs for Stimuli Having Low Depths of Modulation	283
	Leslie R. Bernstein and Constantine Trahiotis	

28	Modeling Physiological and Psychophysical Responses to Precedence Effect Stimuli	293
	Jing Xia, Andrew Brughera, H. Steven Colburn, and Barbara Shinn-Cunningham	
29	Binaurally-Coherent Jitter Improves Neural and Perceptual ITD Sensitivity in Normal and Electric Hearing	303
	M. Goupell, K. Hancock, P. Majdak, B. Laback, and B. Delgutte	
30	Lateralization of Tone Complexes in Noise: The Role of Monaural Envelope Processing in Binaural Hearing	315
	Steven van de Par, Armin Kohlrausch, and Nicolas Le Goff	
31	Adjustment of Interaural-Time-Difference Analysis to Sound Level	325
	Ida Siveke, Christian Leibold, Katharina Kaiser, Benedikt Grothe, and Lutz Wiegrebe	
32	The Role of Envelope Waveform, Adaptation, and Attacks in Binaural Perception	337
	Stephan D. Ewert, Mathias Dietz, Martin Klein-Hennig, and Volker Hohmann	
33	Short-Term Synaptic Plasticity and Adaptation Contribute to the Coding of Timing and Intensity Information	347
	Katrina MacLeod, Go Ashida, Chris Glaze, and Catherine Carr	
34	Adaptive Coding for Auditory Spatial Cues	357
	P. Hehrmann, J.K. Maier, N.S. Harper, D. McAlpine, and Maneesh Sahani	
35	Phase Shifts in Monaural Field Potentials of the Medial Superior Olive	367
	Myles Mc Laughlin, Marcel van der Heijden, and Philip X. Joris	
Part VI Speech Processing and Perception		
36	Representation of Intelligible and Distorted Speech in Human Auditory Cortex	381
	Stefan Uppenkamp and Hagen Wierstorf	

37	Intelligibility of Time-Compressed Speech with Periodic and Aperiodic Insertions of Silence: Evidence for Endogenous Brain Rhythms in Speech Perception?	393
	Oded Ghitza and Steven Greenberg	
38	The Representation of the Pitch of Vowel Sounds in Ferret Auditory Cortex	407
	Jan Schnupp, Andrew King, Kerry Walker, and Jennifer Bizley	
39	Macroscopic and Microscopic Analysis of Speech Recognition in Noise: What Can Be Understood at Which Level?	417
	Thomas Brand, Tim Jürgens, Rainer Beutelmann, Ralf M. Meyer, and Birger Kollmeier	
40	Effects of Peripheral Tuning on the Auditory Nerve's Representation of Speech Envelope and Temporal Fine Structure Cues	429
	Rasha A. Ibrahim and Ian C. Bruce	
41	Room Reflections and Constancy in Speech-Like Sounds: Within-Band Effects	439
	Anthony J. Watkins, Andrew Raimond, and Simon J. Makin	
42	Identification of Perceptual Cues for Consonant Sounds and the Influence of Sensorineural Hearing Loss on Speech Perception	449
	Feipeng Li and Jont B. Allen	
Part VII Auditory Scene Analysis		
43	A Comparative View on the Perception of Mistuning: Constraints of the Auditory Periphery	465
	Astrid Klinge, Naoya Itatani, and Georg M. Klump	
44	Stability of Perceptual Organisation in Auditory Streaming	477
	Susan L. Denham, Kinga Gyimesi, Gábor Stefanics, and István Winkler	
45	Sequential and Simultaneous Auditory Grouping Measured with Synchrony Detection	489
	Christophe Micheyl, Shihab Shamma, Mounya Elhilali, and Andrew J. Oxenham	

46	Rate Versus Temporal Code? A Spatio-Temporal Coherence Model of the Cortical Basis of Streaming	497
	Mounya Elhilali, Ling Ma, Christophe Michey, Andrew Oxenham, and Shihab Shamma	
47	Objective Measures of Auditory Scene Analysis	507
	Robert P. Carlyon, Sarah K. Thompson, Antje Heinrich, Friedemann Pulvermuller, Matthew H. Davis, Yury Shtyrov, Rhodri Cusack, and Ingrid S. Johnsrude	
48	Perception of Concurrent Sentences with Harmonic or Frequency-Shifted Voiced Excitation: Performance of Human Listeners and of Computational Models Based on Autocorrelation	521
	Brian Roberts, Stephen D. Holmes, Christopher J. Darwin, and Guy J. Brown	
Part VIII Novelty Detection, Attention and Learning		
49	Is There Stimulus-Specific Adaptation in the Medial Geniculate Body of the Rat?	535
	Flora M. Antunes, Ellen Covey, and Manuel S. Malmierca	
50	Auditory Streaming at the Cocktail Party: Simultaneous Neural and Behavioral Studies of Auditory Attention	545
	Mounya Elhilali, Juanjuan Xiang, Shihab A. Shamma, and Jonathan Z. Simon	
51	Correlates of Auditory Attention and Task Performance in Primary Auditory and Prefrontal Cortex	555
	Shihab Shamma, Jonathan Fritz, Stephen David, Mounya Elhilali, Daniel Winkowski, and Pingbo Yin	
52	The Implicit Learning of Noise: Behavioral Data and Computational Models	571
	Trevor R. Agus, Marion Beauvais, Simon J. Thorpe, and Daniel Pressnitzer	
53	Role of Primary Auditory Cortex in Acoustic Orientation and Approach-to-Target Responses	581
	Fernando R. Nodal, Victoria M. Bajo, and Andrew J. King	

Part IX Hearing Impairment

54 Objective and Behavioral Estimates of Cochlear Response Times in Normal-Hearing and Hearing-Impaired Human Listeners 597
 Olaf Strelcyk and Torsten Olaf Dau

55 Why Do Hearing-Impaired Listeners Fail to Benefit from Masker Fluctuations? 609
 Joshua G.W. Bernstein

56 Across-Fiber Coding of Temporal Fine-Structure: Effects of Noise-Induced Hearing Loss on Auditory-Nerve Responses 621
 Michael G. Heinz, Jayaganesh Swaminathan, Jonathan D. Boley, and Sushrut Kale

57 Beyond the Audiogram: Identifying and Modeling Patterns of Hearing Deficits 631
 Ray Meddis, Wendy Lecluyse, Christine M. Tan, Manasa R. Panda, and Robert Ferry

Index 641

Chapter 31

Adjustment of Interaural-Time-Difference Analysis to Sound Level

Ida Siveke, Christian Leibold, Katharina Kaiser, Benedikt Grothe, and Lutz Wiegrebe

Abstract To localize low-frequency sound sources in azimuth, the binaural system compares the timing of sound waves at the two ears with microsecond precision. A similarly high precision is also seen in the binaural processing of the envelopes of high-frequency complex sounds. Both for low- and high-frequency sounds, interaural time difference (ITD) acuity is to a large extent independent of sound level. The mechanisms underlying this level-invariant extraction of ITDs by the binaural system are, however, only poorly understood. We use high-frequency pip trains with asymmetric and dichotic pip envelopes in a combined psychophysical, electrophysiological, and modeling approach. Although the dichotic envelopes cannot be physically matched in terms of ITD, the match produced perceptually by humans is very reliable, and it depends systematically on the overall sound level. These data are reflected in neural responses from the gerbil lateral superior olive and lateral lemniscus. The results are predicted in an existing temporal-integration model extended with a level-dependent threshold criterion. These data provide a very sensitive quantification of how the peripheral temporal code is conditioned for binaural analysis.

Keywords Binaural hearing • Loudness • Envelope • Spike timing

31.1 Introduction

Precise temporal coding is the hallmark of the auditory system. Like no other sensory modality, the auditory system relies on the neural analysis of spike timing for both object localization and identification. On the other hand, the peripheral auditory system

L. Wiegrebe (✉)
BioCenter, University of Munich, Munich, Germany
e-mail: wiegrebe@zi.biologie.uni-muenchen.de

has to cope with a huge variability in the loudness of sounds; the dynamic range of natural acoustic input spans at least five orders of magnitude. Psychophysically, it has been shown that sound localization is stable across a wide range of stimulus levels (Blauert 1997). The neural processing underlying this level-invariant encoding of temporal stimulus properties is still poorly understood, in particular since even phase locking, as a basic measure of precise temporal coding, is sensitive to changes in overall sound level in the auditory nerve (Joris et al. 2004). Such level dependence is also seen in the temporal encoding of the envelopes of high-frequency complex tones (Dreyer and Delgutte 2006).

Recent studies on temporal integration of transient sounds have revealed that integration of the stimulus pressure envelope, rather than its intensity can explain both perceptual temporal integration and neural first-spike latency in the auditory nerve at threshold intensity (Heil and Neubauer 2003). It is unclear, however, whether this pressure-envelope integration is sufficient to explain neural integration and how the binaural system uses the temporal response characteristics to form a spatial percept.

In this study, we recruit the binaural system's exquisite temporal sensitivity to quantify temporal integration preceding binaural analysis. We exploit recent findings that interaural time differences (ITDs) of envelopes of high-frequency carriers, "transposed tones," are binaurally analyzed with a precision similar to that of low-frequency tones (Bernstein and Trahiotis 2002, 2003, 2007). At high carrier frequencies, transient stimuli can be constructed which carry different binaural temporal properties although they occupy the same frequency region in the two ears. If the envelopes of these stimuli are binaurally incongruent, the pressure waves cannot be physically matched by simple interaural time shifts. Nevertheless, the binaural system can produce a reliable perceptual match that in turn reflects the way the stimulus envelopes are processed preceding binaural analysis.

31.2 Methods

31.2.1 Psychophysics

31.2.1.1 Stimuli

The current experiments recruit temporally asymmetric pips as illustrated in Fig. 31.1. These pips consist of a high-frequency, pure-tone carrier modulated with a temporally asymmetric envelope. If such a pip is presented binaurally but temporally reversed in one ear, (Fig. 31.1), the pips cannot be physically matched by an ITD. If the sound level is low (Fig. 31.1a), only the tips of the stimulus envelope exceed threshold and consequently, one would expect that the stimulus in the ear with the steeper rise time has to be delayed by an interaural onset difference (IOD) to compensate for the rise-time difference between the ears. If the sound level is high (Fig. 31.1b), the envelope exceeds threshold very quickly and thus, a much smaller IOD would be needed to compensate for the rise-time difference.

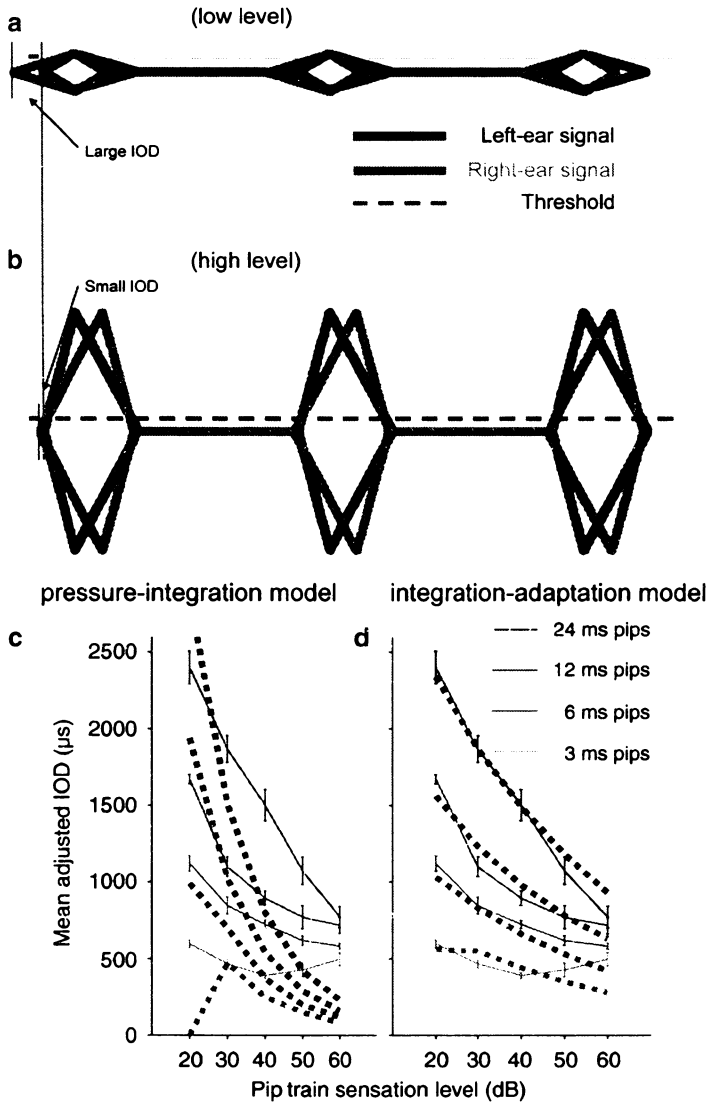


Fig. 31.1 Illustration of the experimental paradigm (a, b) and psychophysical and modeling results (c, d). Listeners were asked to adjust the IOD of binaural pip train to compensate for the interaural differences in the rise- and fall times of the pip envelopes (*black* left ear; *grey* right ear). It is assumed that at low stimulus levels, (a), a large IOD is required for the compensation, whereas at higher levels, (b), smaller IODs are sufficient. The psychophysically adjusted IODs (c, d) confirm this assumption: adjusted IODs systematically decrease with increasing sensation level and decreasing overall pip duration

The used stimuli were trains of such pips with a carrier frequency of 5 kHz. The interval between the pips was fixed at 10 ms. For the left-ear stimuli, the rise time was 1, 2, 4, or 8 ms, and the decay time was always double the rise time, resulting in tone pips

with a duration of 3, 6, 12, or 24 ms. The pip trains in the right ear were either identical to the left-ear trains, or they were temporally reversed. Experiments were run with a continuous background noise (8 dB SPL/Hz) low-pass filtered at 1,500 Hz to preclude the binaural analysis of low-frequency aural distortion products.

31.2.1.2 Procedure

In a two-alternative, forced-choice paradigm without feedback, listeners were asked to judge the lateralization of a test stimulus when compared with a reference stimulus. The reference stimulus was always presented first. It consisted of a diotic pip train with identical rise and decay times in both ears and no IOD. In the standard condition, the test stimulus consisted also of a pip train with identical rise and decay times in the two ears but with an initially randomized IOD between $\pm 500 \mu\text{s}$. In the test condition, the pip train in the right ear was temporally reversed when compared to the left ear. As in the standard condition, listeners were asked to adjust the IOD of these pip trains, which cannot be physically matched to the perceived position of the diotic reference stimulus. In each trial, listeners judged whether the test stimulus was lateralized left or right to the reference stimulus. In an adaptive procedure, the IOD of the test stimulus was changed to compensate for the lateralization of the test stimulus. For the first and second reversal (a change in lateralization direction), IOD was changed in steps of $160 \mu\text{s}$, after the second reversal, the step size was reduced to $80 \mu\text{s}$, and after the fifth reversal, it was reduced to $40 \mu\text{s}$. The adjusted IOD in a given experimental run is given as the mean IOD across reversals six to eleven. Individual data are based on at least six runs per experimental condition. An experimental session consisted of six runs in randomized order, three with temporally reversed test stimuli in the right ear, the other three without reversion. Lateralization was measured as a function of the individually measured pip-train sensation level.

31.2.1.3 Listeners

At least four normal hearing listeners, aged between 21 and 35 of both genders took part in each experiment. Listeners for a pip duration of 6 ms were different from those that acquired all the other data.

31.2.2 Electrophysiology

31.2.2.1 Animals

Recordings were obtained from 18 adult Mongolian gerbils (*Meriones unguiculatus*). Single cells were recorded in two different brainstem nuclei, the LSO ($n=32$) and

the DNLL ($n=66$). All experiments were approved according to the German Tierschutzgesetz (AZ 55.2-1-54-2531-57-05). The detailed methods in terms of surgical preparation, acoustic stimulus delivery, stimulus calibration, and recording techniques have been described previously (Siveke et al. 2006).

31.2.2.2 Recording Procedure and General Neural Characterization

Extracellular single-cell responses were recorded as described earlier (Siveke et al. 2006). The recording sites of 24 of the 32 LSO neurons that we analyzed were histologically verified. Stimuli were generated at 48 kHz sampling rate in Matlab and delivered to the ear-phones (Sony MDR-EX70 LP). Using pure tones, we first determined audio-visually the neuron's characteristic frequency (CF) as that frequency which elicited a response at the lowest intensity, neuronal threshold (thr). For the pip-train experiments, it was first ensured that LSO neurons were IID sensitive, that DNLL neurons were ITD sensitive and that neither phase locked to CF tones.

31.2.2.3 Pip-Train Stimulation

The pips consisted of the same envelopes as in the psychophysical experiments. The carrier frequency was set to the cell's CF. The pips were presented in a 4-s train at a repetition rate of 40 Hz. For the LSO, five repetitions of the pip trains and temporally reversed pip trains were presented monaurally on the ipsilateral ear in a randomized sequence. Pip trains were presented with different pip durations (3, 6, 12, and 24 ms) and different sound levels (18–50 dB above threshold in 8 dB steps).

For the DNLL, the pip trains were presented binaurally: In the contralateral ear the temporal structure of the envelope was constant; in the ipsilateral ear, the stimulation was identical to the LSO monaural stimulation, i.e., the temporal envelope of the pip train was equal to the contralateral side or temporally reversed. Furthermore in the ipsilateral ear, the inter-pip interval was manipulated to generate time-variant envelope ITDs: Within 1 s of pip-train stimulation, the onset of the ipsilateral pip was varied across a range spanning \pm one quarter of the pip duration. This onset range was centered on the best ITD of the neuron. For a 40 Hz pip rate, the ITD range thus consisted of 40 different ITDs. As for the LSO stimulation, pip trains were presented at different pip durations and different sound levels above threshold.

31.2.2.4 Analysis

To calculate the time shift in the period histograms recorded with the standard and time-reversed pips in the LSO, we performed a cross-correlation between the two histograms. A Gaussian was fitted to the cross-correlation function, and the delay at the maximum of the fit was taken as the time shift. For the binaural DNLL

responses, the response rates of the neurons as a function of the IOD were fitted by Gaussians for both standard and ipsilaterally reversed pip trains. The differences between the IODs at which the two Gaussians had their maxima were taken as the IOD change. From the population of recorded neurons ($N=50$), only the neuronal data with a correlation coefficient >0.7 between the data and the Gaussian fits were used for further analysis ($N=30$).

31.3 Results

The IODs adjusted by the listeners to centralize the asymmetric pip trains for the 6-ms pip duration (2 ms rise and 4 ms decay time, or vice versa) are shown with solid lines in Fig. 31.1c. At a sensation level of 20 dB and a pip duration of 24 ms, the listeners adjusted the temporally reversed 24-ms pip train in the right ear (with a 16 ms rise and 8 ms decay time) to start about $2,400\mu\text{s}$ earlier than the pip train in the left ear (with a 8 ms rise and 16 ms decay time). With increasing sensation level, the adjusted IOD decreased monotonically but, even at a high sensation level of 60 dB, the listeners still required an IOD of about $800\mu\text{s}$ to compensate for the temporal reversion and the resulting different rise times in the two ears.

Not surprisingly, the adjusted IOD systematically depended on the overall pip duration. The adjusted IOD decreases with decreasing pip duration for all sensation levels. In all conditions even at the highest tested sensation levels, the adjusted IOD remained above $500\mu\text{s}$.

To study, whether the IOD shifts can be explained by the latency difference $L_l - L_r$, between the left and right-ear evoked neuronal activity, we employed two model variants of the pressure-integration model (Heil and Neubauer 2003). In contrast to the original model, in which latencies are predicted based on the sound pressure wave, we assume integration of the envelope $e(t)$ of the sound pressure wave. Then, the binaural latencies L_l and L_r of action potentials are assumed to be determined by the threshold crossings of the respective integrated envelopes S . Mathematically, this maps to the implicit equation

$$\Theta = S(L_x) = \int_0^{L_x} dt [e_x(t)]^k,$$

in which we allowed an additional exponent k as a fit parameter. In the left model variant (left), the threshold Θ is a constant and independent of sound level. This model thus has two fit parameters, k and Θ . In the second model variant (right), the threshold is a function of the signal level. Specifically, we modeled the threshold as

$$\Theta = \Theta_0 + \Theta_1 \alpha,$$

where α denotes the amplitude of the envelope $e(t)$ in units of Pascal. The second model thus has three fit parameters, k , Θ_0 and Θ_1 .

The model variant with a level independent threshold cannot reproduce the large perceived IODs at high sound levels, although the model qualitatively fits the result in that longer pips produce larger IODs (dashed lines in Fig. 31.1c). In contrast, the model variant that includes a level-dependent threshold can account for the saturation of perceived IODs at high sound levels (dashed lines in Fig. 31.1d).

Neural responses to ipsilateral monaural pip trains from 32 cells with CFs above 2 kHz were obtained from the gerbil LSO. The raster plot (Fig. 31.2b) shows the accurate locking of the cell to the 6 ms pip envelope. The period histograms (2C) show that the spike timing depends on the direction of the asymmetric envelope in that the cell fires earlier when the pip has a 2-ms rise and a 4-ms decay (black). With increasing stimulation level, the response rate increases, but the phase difference between the period histograms of the two envelope conditions decreases. This is quantified in the cross-correlograms of the period histograms in Fig. 31.2d. The peak in the cross-correlogram shifts from $810\mu\text{s}$ at a sound level of 26 dB above threshold to $357\mu\text{s}$ at 50 dB. These main features are preserved in the LSO population average, shown with filled symbols in Fig. 31.2e. Comparable to the psychophysical results, the time shifts extracted from the period histograms decrease with decreasing pip duration and increasing sound level.

Recordings in the DNLL were obtained to get an estimate of how the gerbil's binaural system evaluates the time shifts in the peripheral representation of the pip trains. We systematically searched for high-CF binaural units which showed sensitivity to envelope ITDs in response to Gaussian noise. We used binaural pip trains and introduced a 1-Hz binaural beat into the envelopes of the 4-s pip trains (see Methods). The interaction of this beat with the envelope ITD tuning of a DNLL cell is seen in the raster plot of Fig. 31.3b.

As in all other experiments, we recorded responses both with standard pips in both ears and with ipsilaterally reversed pips (Fig. 31.3a). This stimulation paradigm allows for the evaluation of both phase locking to the pip envelope period (25 ms) and of the binaural locking to the envelope beat period (1,000 ms). As in the LSO, also the DNLL cells locked reliably to the 25 ms period of the pip trains (Fig. 31.3b). Again, the response rates increase with increasing sound level, but this increase was more pronounced for the time-reversed pips (grey), which produced particularly weak responses at low levels. The binaural envelope beat was constructed to cover a range of \pm one quarter of the pip duration within 1 s. Period histograms constructed with the envelope beat period of 1 s are shown in Fig. 31.3c. As within each 1 s period, the envelope IOD changes linearly, the abscissa can be relabeled as an IOD axis. A quantitative analysis of the IOD changes introduced by time reversion of the ipsilateral pips is obtained by fitting a Gaussian to the period histograms in the two conditions and extracting the difference between the fit maxima. The extracted time shifts decrease with increasing sound level (Fig. 31.3d). DNLL population data of the neurally extracted time shifts are shown in Fig. 31.3e. While the DNLL data show qualitatively the same trends as the psychophysical and LSO data, time shifts are significantly smaller than estimated both psychophysically and from the LSO data.

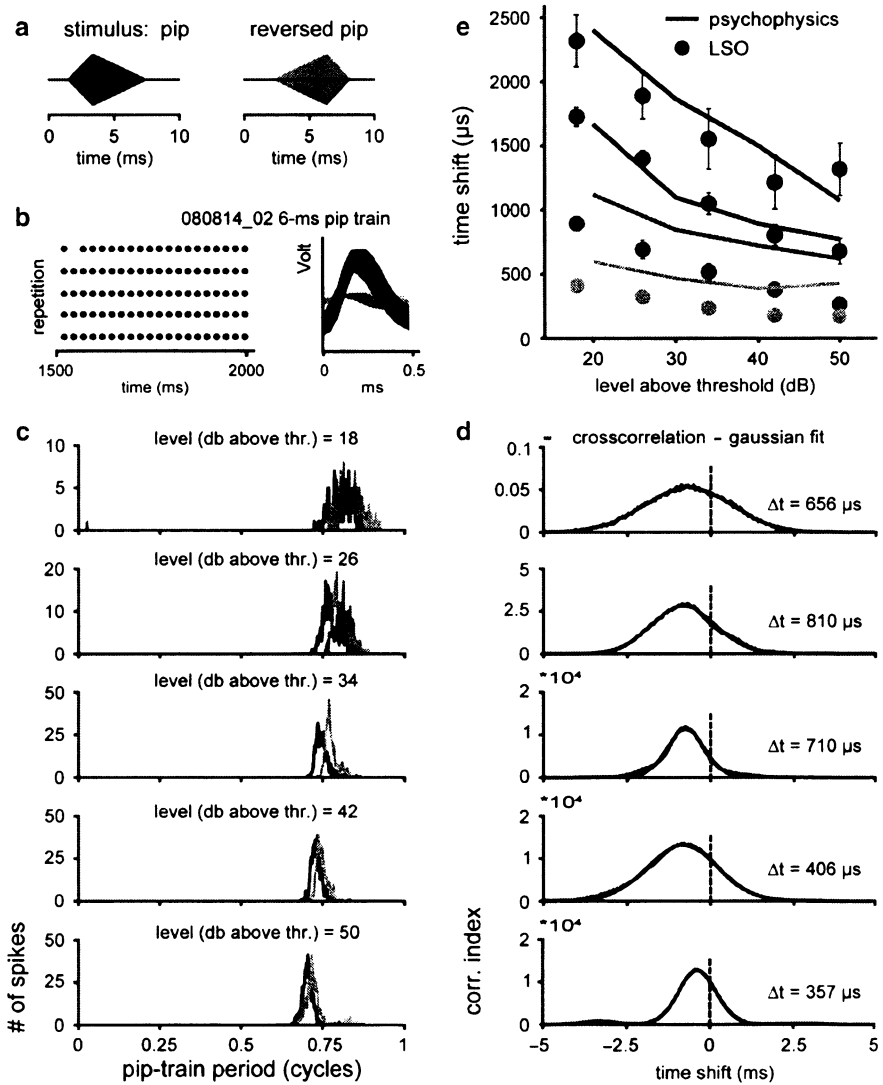


Fig. 31.2 Response of an example LSO neuron (CF=3.5 kHz; thr=20 dB SPL) to monaural pip train stimuli. **(a)** Schematic diagram of the presented standard and the time reversed 6-ms pip. **(b)** Example reaster plot to show the reliable locking of the LSO neuron to the pip-train envelope. **(c)** Period histograms for the standard (*black*) and the time reversed (*grey*) 6-ms pip trains are plotted for five different sound pressure levels ranging from 18 to 50 dB above neuronal threshold. **(d)** cross-correlations of the period histograms are plotted as correlation index versus time shift. The time shift is derived from the time delay (Δt) of the correlation maximum as obtained from a Gaussian fit (*black line*). **(e)** Estimated time shifts from the LSO neural population ($N=32$; *filled symbols*) compared to the psychophysical data (*solid lines*). Estimated time shifts are in good agreement with perceptually adjusted IODs

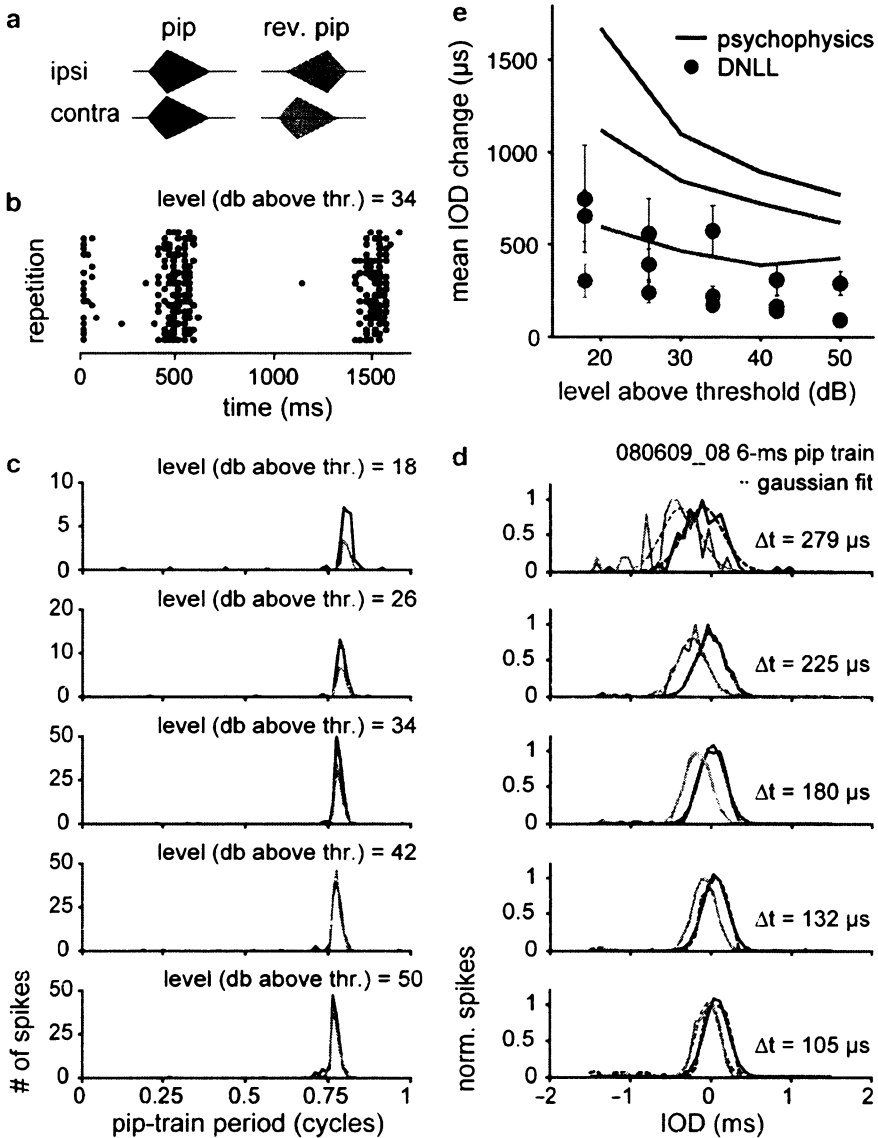


Fig. 31.3 Response of a DNLL neuron (CF=3.6 kHz; thr=25 dB SPL) to the binaural pip train stimuli. The schematic diagram of the presented binaural standard and the time-reversed pips are shown as insets in (a). The raster plot (b) shows a defined acoustical response to a particular envelope IOD of the 6-ms pip train stimuli, which is, according to the “1 Hz beat” stimulation, repeated every second. Period histograms for the standard (black) and the time reversed (grey) 6-ms binaural pips are plotted for five different sound pressure levels ranging from 18 to 50 dB above neuronal threshold in (c). The tuning of the neuron to a particular envelope IOD is revealed by the period histograms constructed with the envelope beat period of 1 s (d). Within each second of the envelope period, the IOD changes linearly, and the abscissa is relabeled as IOD axis. The IOD change (Δt) between the envelope period histograms obtained from the standard (black) and the time reversed pip stimulation is obtained by the difference between the shifts of the two histogram maxima obtained from Gaussian fits (dotted lines). Population data for the time shifts estimated from the binaural stimulation data are shown in (e)

31.4 Discussion

Here, we have presented a binaurally asymmetric stimulus paradigm to investigate the level dependence of ITD processing. The paradigm exploits two key features of auditory processing: the precise encoding of the envelopes of high-frequency carriers and the exquisite precision of ITD analysis. The used pip stimuli are composed of linear up- and downward ramps that constitute the envelope for a sinusoidal high-frequency carrier. The stimuli were investigated with respect to human binaural perception as well as their neuronal representations that are revealed by electrophysiological recordings from the LSO and DNLL of anesthetized gerbils. These three sets of experimental data are in qualitative agreement in that an IOD change induced by the binaural asymmetry of the envelopes increases with signal duration and decreases with signal level.

While the monaurally recorded gerbil LSO data match the human psychophysical data reasonably well, the DNLL data predict much smaller time shifts. Several possible reasons can be envisaged: First, it is conceivable that the recorded monaural LSO responses may not be identical to the inputs of the binaural MSO cells whose output we recorded in the DNLL. Second, to accommodate the large stimulus protocol for the binaural stimulation, a dynamic stimulation paradigm was implemented. Although the acoustic motion introduced by this paradigm is relatively slow, it is conceivable that this dynamic component may interfere with the ITD extraction. Note, however, that time-variant ITDs are encoded with high fidelity in the gerbil DNLL (Siveke et al. 2008). Third, we only inverted the ipsilateral tone pips, but we did not invert the contralateral pips and leave the ipsilateral pips unchanged. These two paradigms would yield the same results if the ipsi- and contralateral inputs converging at the binaural processing stage are identical. If, however, ipsi- and contralateral inputs are not identical (Brand et al. 2002), it is possible that the binaurally observed time shifts depended on whether the ipsi- or contralateral rise time was shallower. This hypothesis remains to be tested.

To check whether the observed IODs can be explained by binaural latency differences, we employed two variants of a temporal integration model by Heil and Neubauer (Heil and Neubauer, 2003; Heil et al. 2007) that was originally proposed to explain the level dependence of the first spike latencies in the auditory nerve. Our experimental data are inconsistent with a simple temporal integration model (Heil and Neubauer 2003). However, including a level dependent threshold into such a model gives a reasonable match between data and model predictions. Heil and Neubauer proposed a neural correlate of their pressure-envelope integration to occur at the inner-hair cell, auditory-nerve synapse. Recent work has addressed the physiological basis of the pressure-envelope integration in the Heil model. In a constructive discourse, it was shown that the interplay between the stochasticity of synaptic events and a short time constant of synaptic transmission can explain the apparently long time constant of temporal integration at threshold (Meddis 2006a, b; Krishna 2006).

The physiological basis for the proposed level-dependent threshold cannot be assessed in the framework of the present study. Our data reveal that this level of adjustment must already be present in the input to the SOC. Dreyer and Delgutte

(2006) showed that at the level of the cat auditory nerve, the temporal representation of transposed tones, with an envelope modulation comparable to the current pip trains, deteriorates with increasing sound level. In contrast, the current data show that at the level of the gerbil LSO, the temporal representation of the pip-train envelopes do not deteriorate with increasing sound level. The current data are thus also in agreement with the psychophysical data showing that sensitivity to envelope ITDs elicited by transposed tones is stable over a wide range of sound levels (Dreyer and Oxenham 2008). These findings argue for a refinement of temporal envelope encoding at the level of the cochlear nucleus, similar to the refinement of phase locking to pure tones (Joris et al. 2004).

Any ITD of the envelope of a high-frequency sound is accompanied by a short-term IID. While it has been shown that IID sensitivity improves with increasing duration (Blauert 1997), the time constant of perceptual IID analysis, i.e., its temporal resolution is entirely unclear. If we assume a long time constant of IID extraction (>20 ms), the IIDs generated by the current stimulation would be negligible. If however, the IID time constant is short, time variant IIDs are generated by the current stimuli. This would be the case for all stimuli with an ITD. To address the question of the time scale of IID processing, it is conceivable to replicate the current psychophysical experiment asking listeners not to compensate the rise-time differences with an ITD but with an IID. Thus, the potential interaction of the current paradigm with IID extraction opens new opportunities to study the dynamics of binaural processing.

Taken together, our experimental paradigm provides insights into the level dependence of binaural processing. Both the perceptual and electrophysiological data can be explained in an existing temporal-integration model extended with a level dependent threshold criterion. These data provide a very sensitive quantification of how the peripheral temporal code is conditioned for binaural analysis.

Acknowledgments The authors would like to thank Alain de Cheveigne and Peter Heil for fruitful suggestions and discussions on the topic. Supported by the DFG and the Bernstein Center for Computational Neuroscience.

References

- Bernstein LR, Trahiotis C (2002) Enhancing sensitivity to interaural delays at high frequencies by using "transposed stimuli". *J Acoust Soc Am* 112:1026–1036
- Bernstein LR, Trahiotis C (2003) Enhancing interaural-delay-based extents of laterality at high frequencies by using "transposed stimuli". *J Acoust Soc Am* 113:3335–3347
- Bernstein LR, Trahiotis C (2007) Why do transposed stimuli enhance binaural processing? Interaural envelope correlation vs envelope normalized fourth moment. *J Acoust Soc Am* 121:EL23–EL28
- Blauert J (1997) *Spatial hearing: the psychophysics of human sound localization*. MIT Press, Cambridge MA
- Brand A, Behrend O, Marquardt T, McAlpine D, Grothe B (2002) Precise inhibition is essential for microsecond interaural time difference coding. *Nature* 417:543–547
- Dreyer A, Delgutte B (2006) Phase locking of auditory-nerve fibers to the envelopes of high-frequency sounds: implications for sound localization. *J Neurophysiol* 96:2327–2341

- Dreyer AA, Oxenham AJ (2008) Effects of level and background noise on interaural time difference discrimination for transposed stimuli. *J Acoust Soc Am* 123:EL1–EL7
- Heil P, Neubauer H (2003) A unifying basis of auditory thresholds based on temporal summation. *Proc Natl Acad Sci U S A* 100:6151–6156
- Heil P, Neubauer H, Irvine DR, Brown M (2007) Spontaneous activity of auditory-nerve fibers: insights into stochastic processes at ribbon synapses. *J Neurosci* 27:8457–8474
- Joris PX, Schreiner CE, Rees A (2004) Neural processing of amplitude-modulated sounds. *Physiol Rev* 84:541–577
- Krishna BS (2006) Comment on “Auditory-nerve first-spike latency and auditory absolute threshold: a computer model” [*J Acoust Soc Am* 119:406–417 (2006)]. *J Acoust Soc Am* 120:591–593
- Meddis R (2006a) Auditory-nerve first-spike latency and auditory absolute threshold: a computer model. *J Acoust Soc Am* 119:406–417
- Meddis R (2006b) Reply to comment on “Auditory-nerve first-spike latency and auditory absolute threshold: a computer model”. *J Acoust Soc Am* 120:1192–1193
- Siveke I, Ewert SD, Grothe B, Wiegand L (2008) Psychophysical and physiological evidence for fast binaural processing. *J Neurosci* 28:2043–2052
- Siveke I, Pecka M, Seidl AH, Baudoux S, Grothe B (2006) Binaural response properties of low-frequency neurons in the gerbil dorsal nucleus of the lateral lemniscus. *J Neurophysiol* 96:1425–1440